


Effect of R load ratio on fatigue crack growth resistance of steels used in automotive applications: experimental results and use of performance prediction models

Leonardo Barbosa Godefroid ^{1*} Américo Tristão Bernardes ¹ Tainan Ferreira Muniz ¹ Jefferson José Vilela ² Fabiano Alcântara Machado ³ 

Abstract

This research consisted in comparing the fatigue crack growth (FCG) performance of four HSLA/ AHSS steels used in automotive applications and with different microstructures, and the application of some prediction models for the da/dN versus ΔK traditional sigmoidal curve as a function of the R load ratio. FCG tests were carried out on C(T) test specimens with R-ratios varying between 0.03 and 0.7. Using the original and empirical methodology proposed by Paris and Erdogan to describe the da/dN - ΔK relationship, the results showed significant differences in function of microstructure, and a deleterious effect of R-ratio increase on the crack growth rate. In order to check existing methodologies based on physical considerations for predicting the fatigue behavior of materials and the effect of the R-ratio mainly in the fatigue threshold ΔK_{th} region, the well-known crack closure model proposed by Elber, an approach using two parameters as a driving force for the crack growth proposed by Vasudevan and co-authors and a combination of these two models recently proposed by Zhu and co-authors were compared. The manifestation of crack closure and its qualitatively expected dependence on the R-ratio were verified for the studied steels, but the Elber model was not able to provide a master curve that accurately summarized the effect of the R-ratio on the sigmoidal fatigue curve of steels. The combined use of two critical thresholds, ΔK_{th}^* and K_{max}^* , for predicting fatigue crack growth according to the Vasudevan model also did not provide accurate results in evaluating the effect of the R-ratio. Regardless of the verified dispersions, there is a connection between the two-parameter methodology and crack closure, hence the model by Zhu and co-authors could be a promising alternative. However, this model also showed significant dispersions and was unable to create a master curve to adequately predict the effect of R-ratio on crack growth. Thus, it can be concluded that this research topic is still open, requiring a more in-depth phenomenological knowledge to predict the effect of the R-ratio on FCG.

Keywords: Fatigue crack growth; Load ratio; Crack closure; Driving force parameters; Steels for automotive industry.

1 Introduction

One of the main challenges of the automotive industry in recent decades is the reduction of the vehicles weight, aiming the new requirements of energy saving and environmental restrictions. Therefore, automobile manufacturers look for materials with conflicting high properties, for example, mechanical tensile strength, formability and fracture toughness, without the need to increase its thickness [1-3]. Steels are commonly used because they meet these characteristics and are in constant development. Ferrite-Bainite (FB) and Ferrite-Martensite (FM) are examples of dual-phase advanced high strength steels (AHSS) widely used in this sector¹ as a substitute for traditional Ferrite-Pearlite (FP) high strength low alloy steels (HSLA).

Due to the type of mechanical loads involved in the use of materials for the automotive industry, research on fatigue crack growth (FCG) has received great attention of the scientific community [4-20]. Studies carried out to estimate the life of a material under fatigue from concepts of Fracture Mechanics provide sigmoidal logarithmical da/dN versus ΔK curves, where da/dN is the FCG rate and $\Delta K (= K_{max} - K_{min})$ is the applied driving force for FCG. One of the first relationships proposed to characterize these curves is due to Paris and Erdogan [21], and is presented in Equation 1. This is the well-known “Paris equation”, which shows a linear trend between da/dN and ΔK , with C and m being constants of the material.

¹ Pós-graduação em Engenharia de Materiais, REDEMAT, Escola de Minas, Universidade Federal de Ouro Preto, UFOP, Ouro Preto, MG, Brasil.

² Centro de Desenvolvimento da Tecnologia Nuclear, CDTN-CNEN, Belo Horizonte, MG, Brasil.

³ MaxionWheels, Limeira, SP, Brasil.

*Corresponding author: leonardo@ufop.edu.br



$$\frac{da}{dN} = C(\Delta K)^m \quad (1)$$

Two deviations are observed in this linear trend. When da/dN approaches to zero, it is possible to determine the threshold stress intensity amplitude, ΔK_{th} , below which there is no crack growth (near-threshold regime). At high ΔK levels, K_{max} approaches to the fracture toughness K_c of the material.

The threshold is an important parameter that characterizes the performance of the materials under fatigue. Chemical composition, microstructure and ferrite grain size noticeably affect the ΔK_{th} value for steels. Dual-phase steels, such as FB and FM, have good resistance to FCG, with greater values of ΔK_{th} in comparison to FP steels. This resistance is attributed to the hard phase (bainite or martensite), which alters the crack path in the ferrite, causing tortuosity and branching, decreasing the driving force and the crack growth rate [4-20].

Since the pioneering work of Paris and Erdogan, the effect of R load ratio (or stress ratio), which is defined as the ratio of minimum to maximum load ($R = P_{min}/P_{max}$), on FCG has been investigated by several researchers. An important procedure is to adapt the cited Paris equation to a relation with a form of Equation 2, where $f(R)$ is an analytical equation including R as a variable.

$$\frac{da}{dN} = C[f(R)\Delta K]^m \quad (2)$$

It has been verified that the FCG is faster at higher R , and more sensitive to R effect when approaching the fatigue threshold ΔK_{th} . As a result, great attention has been paid to the influence of R on FCG behavior in the near-threshold regime in several materials, for example: low alloy steels [22,23], pearlitic steels [24,25], aluminum alloys [26-29], titanium alloys [30,31] and nickel alloys [32-34].

The R -effect on FCG is indeed a valuable matter in designing of materials and structures for engineering applications.

The aim of the research on R -effect is rather simple, that is, to collapse all FCG data at various R into one single “master curve” and find the rules that governing the changing of fatigue strength with R . However, the pathway to the issue is not unique; hence several efforts are based on different points of view.

The concept of crack closure proposed by Elber [35,36] has been reasonably successful in correlating FCG data at various R -ratios. Crack closure results in a decrease in the fatigue driving force ΔK due to, for example, roughness and oxidation of the fracture surface in the near-threshold region (ΔK_{th}) or plasticity at the crack tip in the validity region of the Paris equation. The driving force ΔK is then replaced by an effective stress intensity amplitude, ΔK_{eff} , according to Equation 3. K_{cl} is the stress intensity factor where crack closure occurs and K_{max} is the maximum stress intensity factor. Elber also introduced an effective stress intensity ratio, Equation 4.

$$\Delta K_{eff} = K_{max} - K_{cl} \quad (3)$$

$$U = \frac{\Delta K_{cl}}{\Delta K} = \frac{K_{max} - K_{cl}}{K_{max} - K_{min}} \quad (4)$$

The traditional Paris equation can be then modified to correlate FCG data with R values, as shown in Equation 5. In this equation, C and m are not the same constants of Equation 1. Elber measured the closure stress intensity in a 2024-T3 aluminum alloy at various load levels and R -ratios, and obtained an empirical relationship, Equation 6, then extended for subsequent researchers to various other materials. This method obviously requires the experimental crack closure determination, represented by K_{cl} , and the knowledge of an expression that correlates the crack closure with the R -ratio.

$$\frac{da}{dN} = C(U \Delta K)^m = C(\Delta K_{eff})^m \quad (5)$$

$$U = 0.5 + 0.4R \quad (-0.1 \leq R \leq 0.7) \quad (6)$$

For the highest R ratios, closure was not observed, so $\Delta K = \Delta K_{eff}$. When data at lower R ratios are corrected for closure, the R -ratio effect disappears and all data exhibit the same behavior.

The Elber methodology has generated several adaptations to describe the FCG over the past few decades. For example, according to Hudak and Davidson [37], if ΔK_{th} is related to R this relationship leads to Equation 7, where R^* is the R -ratio above which closure no longer exerts an influence, and ΔK_{th}^* is the ΔK_{eff} for this extreme situation ($\Delta K_{th}^* = U \Delta K_{th}$). Equation 7 predicts that the threshold stress intensity range varies linearly with R below R^* and is constant at higher R ratios. This equation considers that the threshold consists of two components: an extrinsic component that is a function of the R -ratio and is controlled by crack closure ($R \leq R^*$) and an intrinsic component that is a material property independent of crack closure ($R > R^*$). Equation 7 also predicts that for $R = 0$, we have: $\Delta K_{th} = K_{cl} + \Delta K_{th}^*$.

$$\Delta K_{th} = \begin{cases} (K_{cl} + \Delta K_{th}^*)(1 - R) & R \leq R^* \\ \Delta K_{th}^* & R > R^* \end{cases} \quad (7)$$

In a different point of view, Vasudevan et al. [38-42] have proposed a two-parameter driving force approach where ΔK and K_{max} are both required to FCG, without invoking crack closure. In this methodology, two critical intrinsic thresholds, ΔK_{th}^* and K_{max}^* , need to be reached simultaneously to start the FCG. They point out that their approach is analogous to the “Goodman diagram” for $S-N$ curves, where fatigue life is a function of both stress amplitude and mean stress. Once it is recognized that there are two driving forces for fatigue crack growth, it becomes more appropriated to

represent fatigue crack growth rate, da/dN , in terms of a three-dimensional (3D) plot as a function of ΔK , and K_{max} . However, a more convenient 2D representation of 3D behavior can be obtained if cuts perpendicular to the da/dN axis are taken. This methodology generates an “L-shaped” threshold curve that can be considered as a fatigue map: it represents an interplay of the two driving forces needed to enforce a given crack growth rate. As the two threshold values from the model of Vasudevan change with the da/dN crack growth rate, then a crack growth “trajectory map” can be defined following the changes of ΔK and K_{max} as a function of da/dN . These maps then reflect the material resistance to crack growth and changes in the trajectory (more than one L-shape curve for the same da/dN) correspond to changes in the mechanism that controls the FCG.

According to Anderson [20], it is interesting to note that when the “L-shaped” curve is plotted as ΔK_{th} versus R , the resulting trend is similar to the crack closure theory that can be expressed mathematically by Equation 7, where $K_{cl} + \Delta K_{th}^* = K_{max}^*$ [20,37]. Therefore, the existence of thresholds for both K_{max} and ΔK can be considered wholly consistent with the closure argument, although Vasudevan and his colleagues insist on disagreeing with this reasoning. They insist that the two parameters ΔK_{th}^* and K_{max}^* are intrinsic characteristics of the material, and that the FCG does not occur simply because of an extrinsic factor like the crack closure.

In a recent research by Zhu et al. [43,44], the application of these two approaches previously mentioned independently to R -effect in the near-threshold fatigue regime (Elber and Vasudevan) is observed to be either shortage of accuracy or full of uncertainties, as a result of the complexities and difficulties in both experimental measurement and modeling key parameters in the case of the procedure used to generate the near-threshold region. One possible solution to this issue is to take both the two approaches into account by using a suitable merging technique considering both ΔK_{eff} and K_{max} parameters.

Zhu et al. [43,44] investigated the R -effect on FCG, combined the crack closure concept and the two-parameters approach method. They also considered a new crack opening equation, without involving crack closure measurement, and an equation relating the crack growth rate da/dN to the driving force ΔK in the near-threshold regime (ΔK_{th}), based on several values for the R -ratio. This new model assumes the existence of the crack closure, however only influencing the FCG below a certain value for the R . In other words, there is a particular value of R , here called R_c (the same physical meaning of R^* of the crack closure model), above which the crack closure will have no influence on the FCG. A general FCG equation in the form of the Paris equation, $da/dN = C[A(R)\Delta K^{B(R)}]^m$, was put forward for the near-threshold FCG, which was reasonably used to predict the R dependence of FCG curve and fatigue threshold, with the C and m constants valid only for this region. This FCG equation was further validated using FCG data in the open

literatures and believed to be eligible and suitable to predict fatigue thresholds in a variety of Cr–Mo–V steels.

The methodology proposed by Zhu et al. [43,44] requires an FCG test with a relatively high R value (reference value), when there is no influence of crack closure. The generated curve da/dN versus ΔK in the threshold region gives reference values for the driving force ΔK_{ref} . From these reference data, values of $(da/dN)_R$ and $(\Delta K)_R$ are obtained for any value of R , using Equation 8 and Equation 9, respectively, and the material-specific analytical equations A and B including R as a variable, provided by Equations 10 and 11.

$$\left(\frac{da}{dN}\right)_R = C \left(\frac{1}{A(R)} \cdot \left(\Delta K_{ref}^{(1-b(R))} \right) \right)^m \quad (8)$$

$$(\Delta K)_R = \frac{1}{A(R)} \cdot \Delta K_{ref}^{(1-B(R))} \quad (9)$$

$$A(R) = a_2 R^2 + b_2 R + c_2 \quad (10)$$

$$B(R) = a_3 R + b_3 \quad (11)$$

Considering the importance of an adequate selection of steels for the current context of the automobile industry, which searches for the use of materials with reduced weight and increased mechanical properties, and also considering the importance of having an accurate prediction model of fatigue life of these materials, this research consisted in comparing the fatigue crack growth performance of four HSLA/AHSS steels, with different microstructures (ferrite/pearlite, ferrite/pearlite/bainite, ferrite/bainite and ferrite/martensite), and the application of some prediction models for da/dN versus ΔK curve as a function of the R load ratio mainly in the region of the threshold ΔK_{th} .

2 Materials and methodology

Four hot rolled low carbon steels were received from a Brazilian company specializing in the stamping of automotive components. The materials were identified as S1, S2, S3 and S4. Their chemical composition, determined by optical emission spectrometry (OES), is presented in Table 1. S1 is a HSLA modified AISI 1010 grade steel, with a ferrite-pearlite microstructure. S2 is a HSLA niobium microalloyed steel, with ferrite-pearlite microstructure. S3 and S4 are AHSS dual-phase ferrite-bainite and ferrite martensite steels, respectively, being the first a niobium microalloyed and the second a high chromium steel.

The samples used for microstructural examination were cut, ground, polished and etched with a special solution (picral and after Na-metabisulfite) developed to reveal microconstituents of high strength steels [45]. The samples were examined using a LEICA light optical microscope (LOM) and a TESCAN VEGA3 scanning electron microscope

Table 1. Chemical composition of the studied steels (wt%)

Steel	C	Si	Mn	P	S	Nb	Cr	Ni	Mo	N
S1	0.08	0.02	0.36	0.02	0.007	0.003	0.003	0.001	0.01	0.0037
S2	0.08	0.03	0.65	0.02	0.007	0.033	0.002	0.007	0.01	0.0039
S3	0.05	0.02	1.79	0.03	0.003	0.035	0.003	0.01	0.03	0.0068
S4	0.05	0.01	1.42	0.06	0.003	0.007	0.470	0.01	0.02	0.0073

(SEM). The corresponding ferrite grain size of each steel was measured according to the standard ASTM E112 [46].

Tensile properties of the steels were obtained according to the standard ASTM E8 M [47] on a 100kN 5882 Instron electro-mechanical system interfaced to a computer for machine control and data acquisition. Three specimens are considered for each steel. The Vickers hardness was obtained according to the standard ASTM E92 [48].

All the FCG tests were performed on a 100kN 8802 Instron servo-hydraulic materials testing system interfaced to a computer for machine control and data acquisition, at room temperature in atmospheric air. The tests were conducted under a sinusoidal waveform with a frequency of 35Hz, in accordance with the recommendations of ASTM E647 [49].

Compact tension C(T) specimens oriented in T-L direction were considered for each steel, with 3mm thickness, 50mm width and a fatigue pre-crack length of 3mm to have an initial crack size to width ratio (a/W) of 0.26. Crack opening displacement (COD) measurements were performed using a COD extensometer and crack size evaluation was performed using the compliance method. Crack size curves in function of the number of cycles have been obtained and transformed to crack growth rate curves (da/dN) as a function of cyclic stress intensity factor (ΔK). Five R -ratio are considered: $R = 0.03, 0.1, 0.4, 0.5$ and 0.7 . The fatigue threshold value ΔK_{th} was defined as the stress intensity factor range at which the fatigue crack growth rate decreased to below 1×10^{-7} mm/cycle. This value was estimated by a K -decreasing procedure (load-shedding process), limiting the normalized K -gradient, $C = (I/K)$. (dK/da) to -0.08mm^{-1} . ΔK_{th} was obtained from the best-fit straight line from a linear regression of $\log da/dN$ versus $\log \Delta K$ between growth rates of 10^{-6} and 10^{-7} mm/cycle.

Closure measurements for the application of the Elber model [35,36] were calculated for many crack sizes at the threshold region through the compliance technique, where a change of linearity was formed in the applied load versus COD curve. With K_{cl} calculated, Equation 5 was applied in order to obtain the “master curve” da/dN versus ΔK_{eff} for the four studied steels. Equations of the type of Equation 6 were obtained with the experimental results, to know the dependence of the effective stress intensity ratio with the R -ratio. This methodology served to find a particular value for the R -ratio, above which the crack closure is not observed, an important result to be used in the subsequent models analyzed.

The values of ΔK and K_{max} used in the Vasudevan et al. [38-42] methodology for the FGC rate of 1×10^{-7} mm/cycles were

plotted in graphs for the identification of the critical values that allow the FCG. In this way, the values of ΔK_{th}^* and $K_{max,th}^*$ were obtained for all studied steels. Equation 12 was used to increase the amount of data at the rate of 1×10^{-7} mm cycle, where the parameter K_0 represents the ΔK_{th} value for $R = 0$ and γ is an adjustment constant between 0 and 1 [50].

$$K_0 = \frac{\Delta K_{th}}{(1-R)^\gamma} \quad (12)$$

Still exploring the concepts adopted by Vasudevan and with the obtained value of R^* , graphs of ΔK versus R were traced to verify the validity of Equation 7 and to analysis the possible existence of a connection between this model and crack closure.

With the adopted value of R_c ($R_c = R^*$), the methodology of Zhu et al. [43,44] was applied. For six specific da/dN values, graphs were plotted between $\ln \Delta K$ and $(2R/(1-R))$ for different R and the slope of each line (α) was taken. When R is less than R_c , α is called α_1 , otherwise α is equal to α_2 . For each test performed with different R , the Paris equation was applied to the region of ΔK_{th} with the correction for ΔK according to Equation 13 and the constants C_0 and m_0 were obtained. From the parameters C_0 , m_0 , α_1 and α_2 , the crack closure coefficient $U_{(R)}$ is obtained by Equation 14 and later simplified in Equation 15.

With this information it can use Equation 8 to Equation 11, to predict the fatigue crack growth in the near-threshold regime for different values of R .

$$\Delta K_0 = \Delta K_R \exp\left(\alpha \frac{2R}{1-R}\right) \quad (13)$$

$$U_{(R)} = \frac{\left(\frac{C_{0(R)}}{C_{0(ref)}}\right)^{1/m_{0(R)}}}{\exp\left(18\alpha_2 - \alpha \frac{2R}{1-R}\right)} \left(\Delta K_{0(ref)}\right)^{1-m_{0(ref)}/m_{0(R)}} \quad (14)$$

$$U_{(R)} = A(R) \cdot \Delta K_{ref}^{B(R)} \quad (15)$$

3 Results and discussion

3.1 Comparison among the steels performance

Figure 1 shows the microstructures of the four studied steels. The S1 steel contains a microstructure composed of

equiaxial and relatively coarse grains of ferrite and colonies of fine pearlite. The microstructure of the S2 steel consists of elongated and finer grains of ferrite and pearlite colonies. A small volume fraction of bainite is also observed. A very refined structure is observed in S3 steel, constituted by elongated grains of ferrite and bainite. An equiaxial and refined microstructure is observed in S4 steel, formed by martensite islands surrounded by a ferritic matrix. These different microstructures result from the different chemical compositions and also from the different thermo-mechanical rolling procedures applied in the steels [1-3].

The ferritic grain size of each material and the volume fractions of the phases/constituents are shown in Table 2. It is confirmed that all steels are ferritic with small amounts of other phases/constituents, and that S3 steel has the most refined structure among the studied steels. The values found for volume fraction of the phases/constituents agree with values commonly used in steels for the automotive industry [1-3]. It is interesting to note that up to a certain value of martensite volume fraction, usually 50%, the value of the threshold ΔK_{th} will tend to increase, according to literature data⁴⁻¹⁹, improving the fatigue resistance of the

material. However, these high values of martensite cannot be industrially considered, due to operational losses in the stamping stage for the manufacture of automotive components.

Table 3 summarizes the main tensile results and also hardness values. The values of tensile strength, strain-hardening coefficient and strain to fracture are in accordance with the classification for HSLA and AHSS steels used in the automotive industry [1,51].

It can be seen an inverse relation between the mechanical strength and the ductility of the steels, due the presence of different phases/constituents, elements in solid solution, precipitates and ferritic grain size [52-55].

The S2, S3 and S4 steels presented a similar fracture energy (U parameter estimated by the area below the tensile curves, and shown in Table 3), superior to the S1 steel. The S4 steel has a lower yield strength than the other steels but, because of a higher strain-hardening capacity, reaches the higher ultimate tensile strength. The strain hardening and high strength of DP steels are a result of martensite formation. Hard martensite regions in ferrite provide dispersion strengthening according to the rule of mixtures, i.e., the more martensite, the greater the strengthening, but also introduce

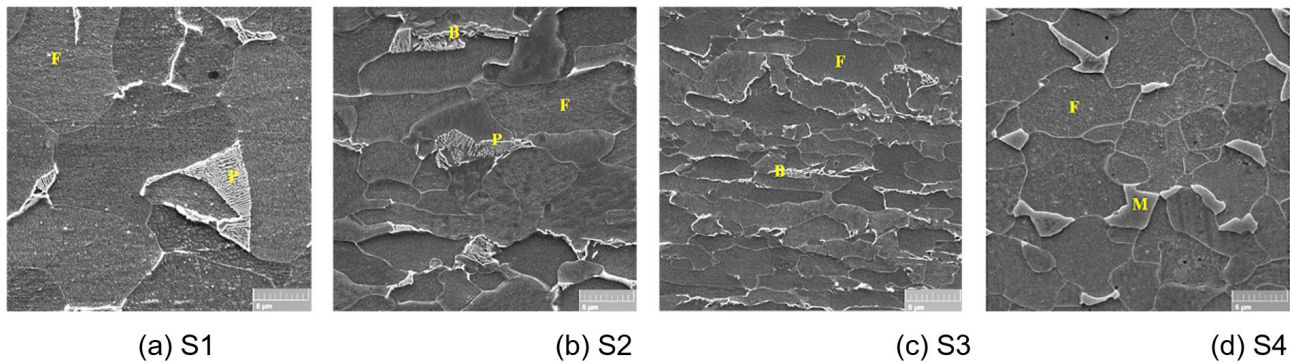


Figure 1. SEM micrographs of the steels, etched with picral and Na-metabisulfite solutions [45]. F = ferrite; P = pearlite; B = bainite; M = martensite.

Table 2. Ferritic grain size and phase/constituents volume fraction

Steel	ASTM grain size	FVF (%)	PVF (%)	BVF (%)	MVF (%)
S1	11 ± 0.4	92.7 ± 0.5	7.3 ± 0.5	-	-
S2	13 ± 0.3	92.5 ± 2.6	4.5 ± 2.0	3.0 ± 1.0	-
S3	14 ± 0.7	92.0 ± 0.5	-	8.0 ± 0.5	-
S4	13 ± 0.3	86.0 ± 1.7	-	-	14.0 ± 1.7

FVF = ferrite volume fraction; PVF = pearlite volume fraction; BVF = bainite volume fraction; MVF = martensite volume fraction.

Table 3. Tensile properties and hardness of the steels

Steel	YS (MPa)	UTS (MPa)	DEF (%)	AR (%)	n	U (MPa)	HV
S1	265 ± 35	350 ± 34	44 ± 2	68 ± 2	0.18	143	124 ± 2
S2	423 ± 2	493 ± 5	42 ± 3	63 ± 3	0.20	196	180 ± 14
S3	493 ± 9	548 ± 6	35 ± 2	59 ± 4	0.15	181	188 ± 3
S4	402 ± 7	636 ± 8	31 ± 1	52 ± 2	0.21	182	203 ± 2

YS: Yield Strength; UTS: Ultimate Tensile Strength; DEF: Strain for fracture; AR: area reduction; n: strain-hardening coefficient; U: absorbed energy; HV: Vickers Hardness.

high densities of dislocations into the ferrite around the martensite. In the ferrite adjacent to the martensite there is a very high density of dislocations. These dislocations are generated by the shear and volume changes associated with the transformation of austenite to martensite. Dislocation densities are much lower in the ferrite removed from the martensite islands. The dislocations around the martensite are not pinned and account for the absence of the discontinuous yielding (no sharp yield point) exhibited in mild steels and HSLA steels. The martensite-induced dislocations move at low stresses, creating low yield strengths, and interact to produce high rates of strain hardening [56-60]. Independently of the differences in mechanical properties of the steels, all tensile specimens presented a ductile behavior, with operation of the mechanism of nucleation, growth and coalescence of microcavities. The dimples had the smallest size in S3 steel, due to its smaller grain size.

The sigmoidal da/dN versus ΔK curves for the four steels, with $R = 0.1$, are presented in Figure 2. It is possible to see the three different regions of FCG commonly found in metals. When comparing the fatigue behavior of the steels, it is observed that they have similar behavior in the linear Region II (Paris's equation), since this region is less sensitive to chemical composition and microstructure. In region I and region III, there is a significant different behavior among the steels, since the FCG in these regions is strongly influenced by the chemical composition and the microstructure of the material [5,6,9-11,15]. The S3 presented the highest value of ΔK_{th} , having, then, the best fatigue performance among the materials, followed by S4 steel. The best performance of AHSS steels is reported in the literature³ as a consequence of the presence of the dual-phase microstructure, i.e., bainite or martensite in a ferritic matrix. In this case, the FCG in the ferrite will create tortuosity and bifurcation when the crack encounters the hardest phase, the driving force decreases and the FCG rate decreases.

Figure 3 shows the fracture surfaces of fatigued specimens for $R = 0.1$. For each steel considered, the fracture

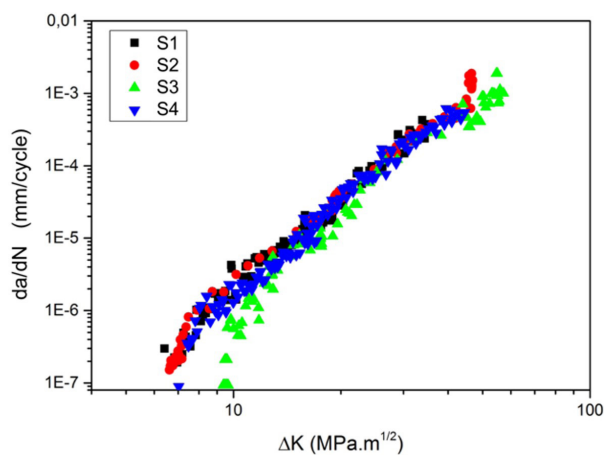


Figure 2. Sigmoidal curves da/dN versus ΔK with $R = 0.1$ for all studied steels.

surface was analyzed for two da/dN crack growth rates, 1×10^{-7} and 5×10^{-5} mm/cycle, which correspond, respectively, to the beginning of region I (crack growth threshold) and region II (linear region between da/dN and ΔK). For all steels the fatigue fracture surface presented at the near-threshold region a predominant transgranular fracture mode, with the “hill-and-valley” type appearance and shear facets, with an associated zig-zag path primarily through the ferrite. Such fractures show high linear roughness and high crack deflection angles. At higher growth rates, characteristics of region II, fracture surfaces remain transgranular, but with evidence of striations. These fracture mechanisms did not change with the change in the value of R . All these fractographic characteristics are found in many materials [6,15,17,22,25].

The deleterious effect of increased R -ratio on the ΔK_{th} is showed in Table 4 for all the studied steels, as expected and reported in the literature (researches cited in the introduction of this article) for several materials. When considering the performance of each steel, S3 and S4 presents better behavior in the values of ΔK_{th} . The presence of bainite/martensite in these microstructures justifies again such behavior [9,11,15].

From the set of mechanical properties evaluated, it can be concluded that the two AHSS grade steels are superior to the two HSLA steels. The following applied models should therefore predict this performance.

3.2 Application of the Elber model

Figure 4 shows the da/dN versus ΔK and da/dN versus ΔK_{eff} curves using the Elber concept of crack closure for each steel studied. The deviation of the linearity of the curve $P \times COD$ was evaluated to verify the presence of crack closure in the performed tests. The existence of crack closure was precisely observed for R equal to 0.03, 0.1 and 0.4 and completely absent for R equal to 0.7. Thus, the value $R = 0.7$ was adopted for R^* and R_c used in the subsequent models. It's interesting to remember that, as remarked in the introduction of the article, R^* (adaptation of Elber's model, proposed by Hudak and Davidson) has the same physical and numerical meaning as R_c (proposed by Zhu and coauthors' model).

It is observed that the curves for different values of R tend to overlap when ΔK is “corrected” to ΔK_{eff} , generating a “master curve” for the material. However, it is important to observe that it exists a certain dispersion (33% maximum) in an attempt to trace the “master curve” in the near-threshold region. This dispersion can be related to the experimental determination of the crack closure, that is affected by existing

Table 4. Effect of R -ratio on the fatigue threshold ΔK_{th} for the studied steels

Steel	R = 0.03	R = 0.1	R = 0.4	R = 0.5	R = 0.7
S1	6.7	6.2	6.3	-	3.9
S2	5.8	6.6	-	5.2	4.3
S3	6.0	9.5	-	5.3	3.9
S4	7.7	7.0	6.9	-	5.7

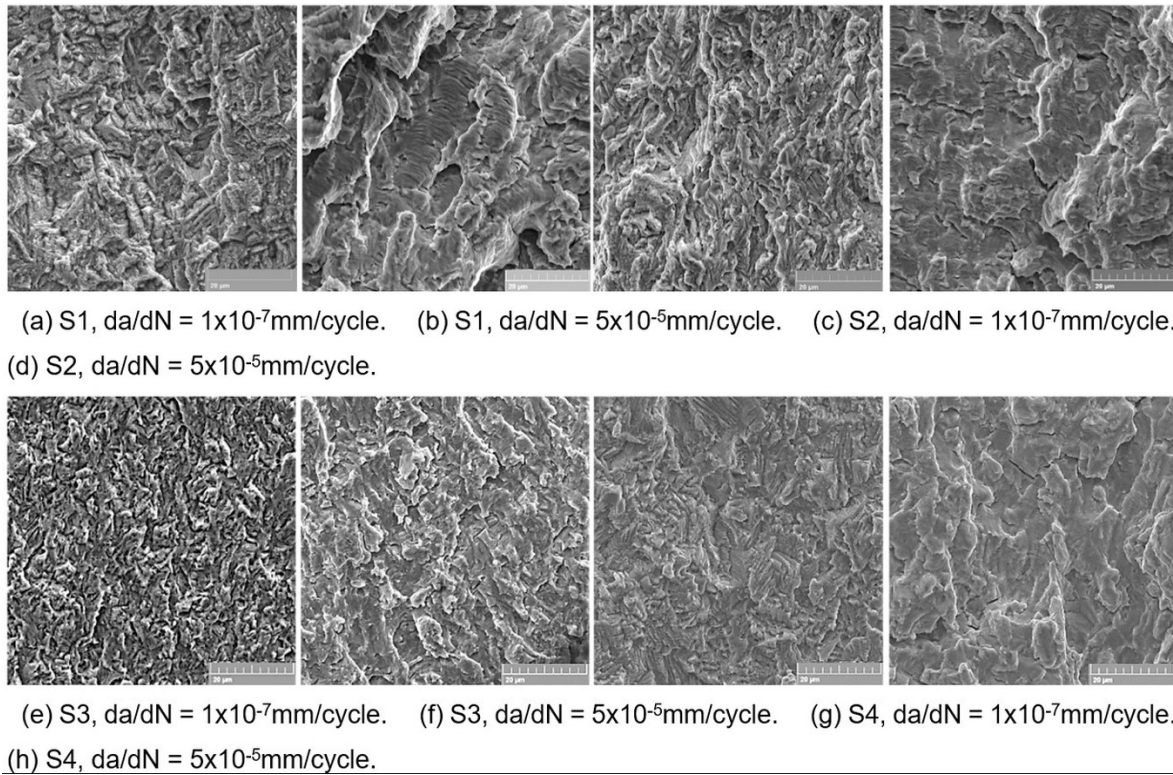


Figure 3. SEM fractographies of fatigued specimens.

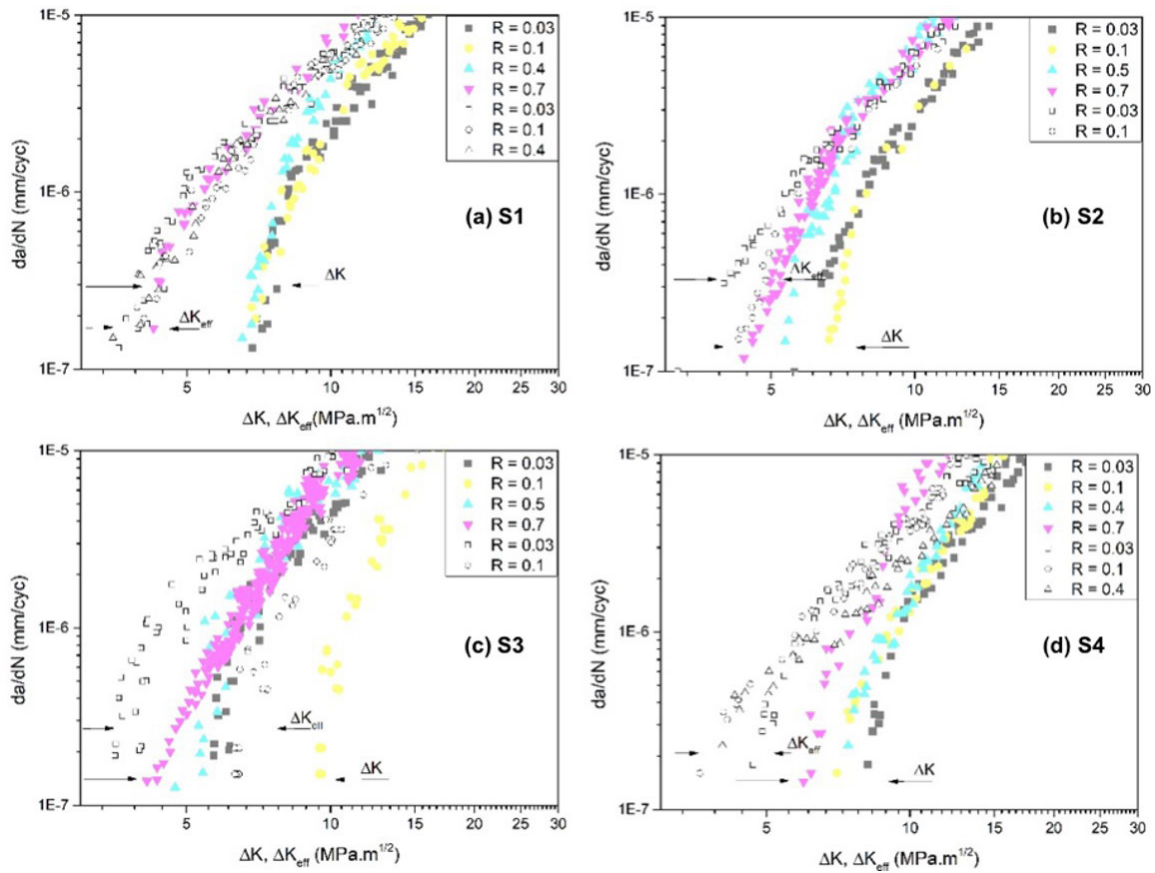


Figure 4. da/dN versus ΔK (filled dots) and da/dN versus ΔK_{eff} (open dots) for all R ratio. Elber's model.

different threshold testing methods and crack growth shielding mechanisms. It can also be argued that the crack closure could not be the unique agent controlling the FCG in this region, according to the ideas of Vasudevan and co-authors. This subject will be discussed later.

Table 5 shows a comparison between values of ΔK_{th} and ΔK_{eff} . It is observed a reduction in the value of ΔK_{th} that occurs when it is corrected for ΔK_{eff} due to the effect of crack closure. It was observed that the crack closure U coefficient varies with R following the form of a linear equation, similar to Equation 6. Table 6 presents the intercept and the slope of the equations for all steels.

To better analyze the conjecture of curves overlapping in the Elber model, it was performed a linear fit to $\log(da/dn) = C' + m \log(\Delta K_{eff})$. The results are shown in Figure 5. It was also plotted the confidence bands and projection bands. A confidence level of 95% was defined, which is usual in this kind of analysis. Projection bands are used to confirm the basic assumption of curves overlapping.

Table 5. Effect of crack closure on ΔK_{th} (MPa.m^{1/2}). Elber's model

Steel	R				
	0.03	0.1	0.4	0.5	0.7
S1 $\Delta K_{th} / \Delta K_{eff}$	6.7/3.7	6.2/3.6	6.3/3.4	-	3.9/3.9
S2 $\Delta K_{th} / \Delta K_{eff}$	5.8/3.2	6.6/4.1	-	5.2/5.2	4.3/4.3
S3 $\Delta K_{th} / \Delta K_{eff}$	6.0/3.7	9.5/6.1	-	5.3/5.3	3.9/3.9
S4 $\Delta K_{th} / \Delta K_{eff}$	7.7/4.6	7.0/3.6	6.9/3.8	-	5.7/5.7

Table 6. Parameters of linear equation of crack closure U coefficient ($U = a_1 + b_1 R$)

Steel	a_1	b_1
S1	0.56807	-0.05289
S2	0.53051	0.95061
S3	0.55048	2.09524
S4	0.56431	-0.08078

For S1 sample, the coefficient of determination R^2 is ~ 0.95 , which represents a good fitting. It is observed that most of the adjusted points to ΔK_{eff} are included within the prediction bands, reinforcing the conjecture of overlap. The residuals analysis shows a distribution which can be interpreted either a signal of outliers or the existence of a changing behavior (discussed below in this text). For S2 it is observed the same behavior as that of S1: most of “normalized” points are within the prediction bands and the residuals histogram shows the presence of outliers or a changing behavior. This assumption will be better discussed below. However, for S3 and S4, most of the normalized points are outside the prediction bands, as one can see in the Figure 5. Although the coefficient of determination R^2 is close to 0.9 for both cases, the results do not support the basic assumption of measurements overlapping. In both cases, the dispersion of data is greater than in previous S1 and S2 cases, as one can observe in the residual plots.

3.3 Application of the Vasudevan model

The fundamental threshold curves were constructed from the data of ΔK_{th} and K_{max} using experimental data for the four steels studied and predicted results obtained from Equation 12, as show in Figure 6. The data of all the materials result in curves with an L-shape, as was expected by this methodology. It is possible to define values of ΔK^* and K_{max}^* where the FCG rate is close to zero. These two parameters are considered thresholds, ΔK_{th}^* and $K_{max,th}^*$ because the data were taken for $da/dN = 1 \times 10^{-7}$ mm/cycle. Table 7 presents these values for each steel. It is important to observe that it also exists a certain dispersion of results. F-tests have been performed to compare the two datasets of each steel (results obtained experimentally with results calculated from the theoretical model). In all the cases, for a significance level of 0.5, the sets are statistically different. This dispersion may come from the use of Equation 12, which

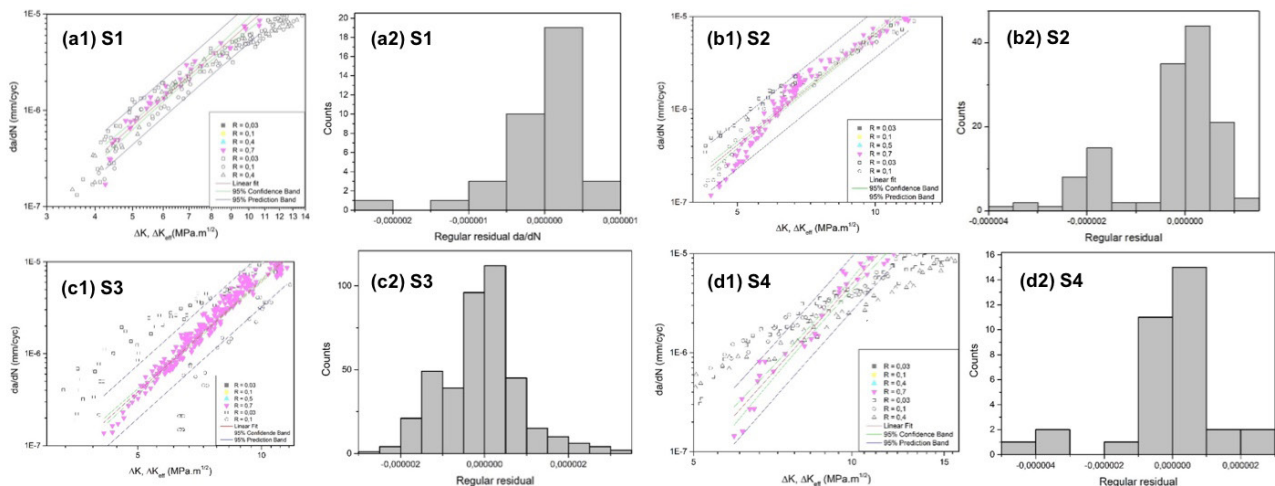


Figure 5. Linear Regression and residuals for linear regression. Elber's model.

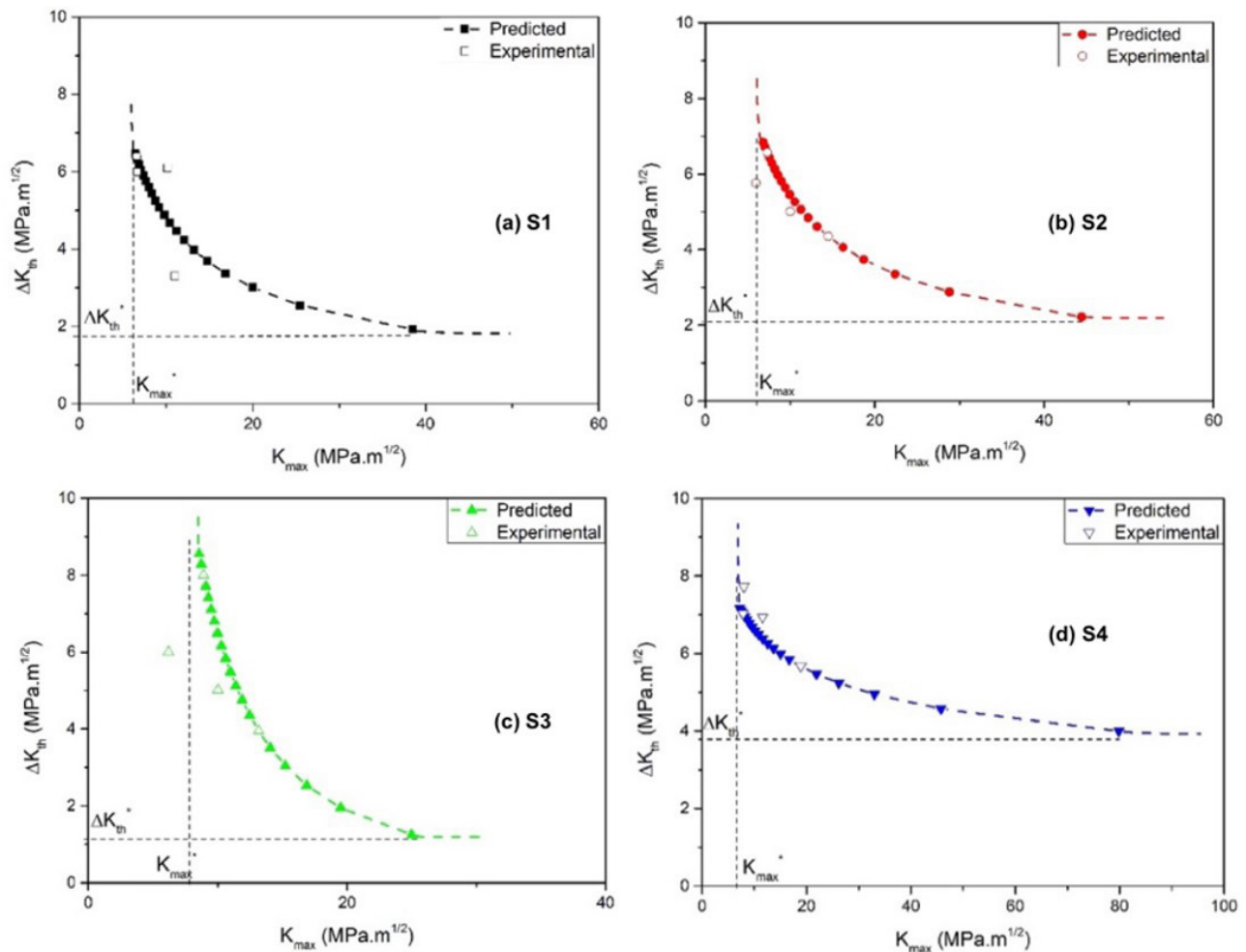


Figure 6. ΔK_{th} and K_{max} curves. Vasudevan’s model.

Table 7. Values of ΔK_{th}^* and $K_{max,th}^*$ for each steel

Steel	ΔK_{th}^* (MPa.m ^{1/2})	$K_{max,th}^*$ (MPa.m ^{1/2})
S1	2.4	6.4
S2	2.2	6.3
S3	1.9	7.8
S4	3.9	7.2

Vasudevan and co-authors model.

would require an adaptation. Another alternative would be to carry out a larger number of tests, using more R values to improve the accuracy.

Figure 7 shows ΔK_{th} versus R curves obtained from experimental results. For all steels, $R^* = 0.7$ was considered, according to the experimental results commented on the application of the Elber model. It is noted that these curves show a similar trend to the curves proposed by Hudak and Davidson [37] which consider crack closure as an extrinsic phenomenon that controls FCG. Thus, it is possible to argue that the existence of two thresholds for driving force, ΔK_{th} and K_{max} , are consistent with the crack closure effect. There is then a connection between the two parameters’ methodology

and the crack closure. However, when trying to complete Figure 7 with ΔK_{th} values predicted by Equation 12, one can see that there is a reasonable dispersion of results. Thus, it is possible to confirm that this equation is not accurate to be used to represent the FCG.

The values of the ΔK_{th}^* and $K_{max,th}^*$ thresholds for each material, taken from Figure 6 and according to Equation 7, are presented in Table 8. A considerable difference between these values and those presented by Table 7 (Vasudevan’s model) is observed. By adopting Vasudevan and co-authors’ model, it can already be seen that the two S3 and S4 AHSS steels would be the materials with the greatest resistance to fatigue cracking.

On the other hand, the analysis that considers the crack closure operation indicates that S4 steel is the most appropriate steel among the analyzed materials. Although the Vasudevan’s model has the advantage of dispensing the experimental measurement of crack closure, this phenomenon was verified and its use in predicting fatigue behavior leads to a better precision in the selection of materials.

Therefore, it is always important to consider an analysis that takes crack closure into account. However,

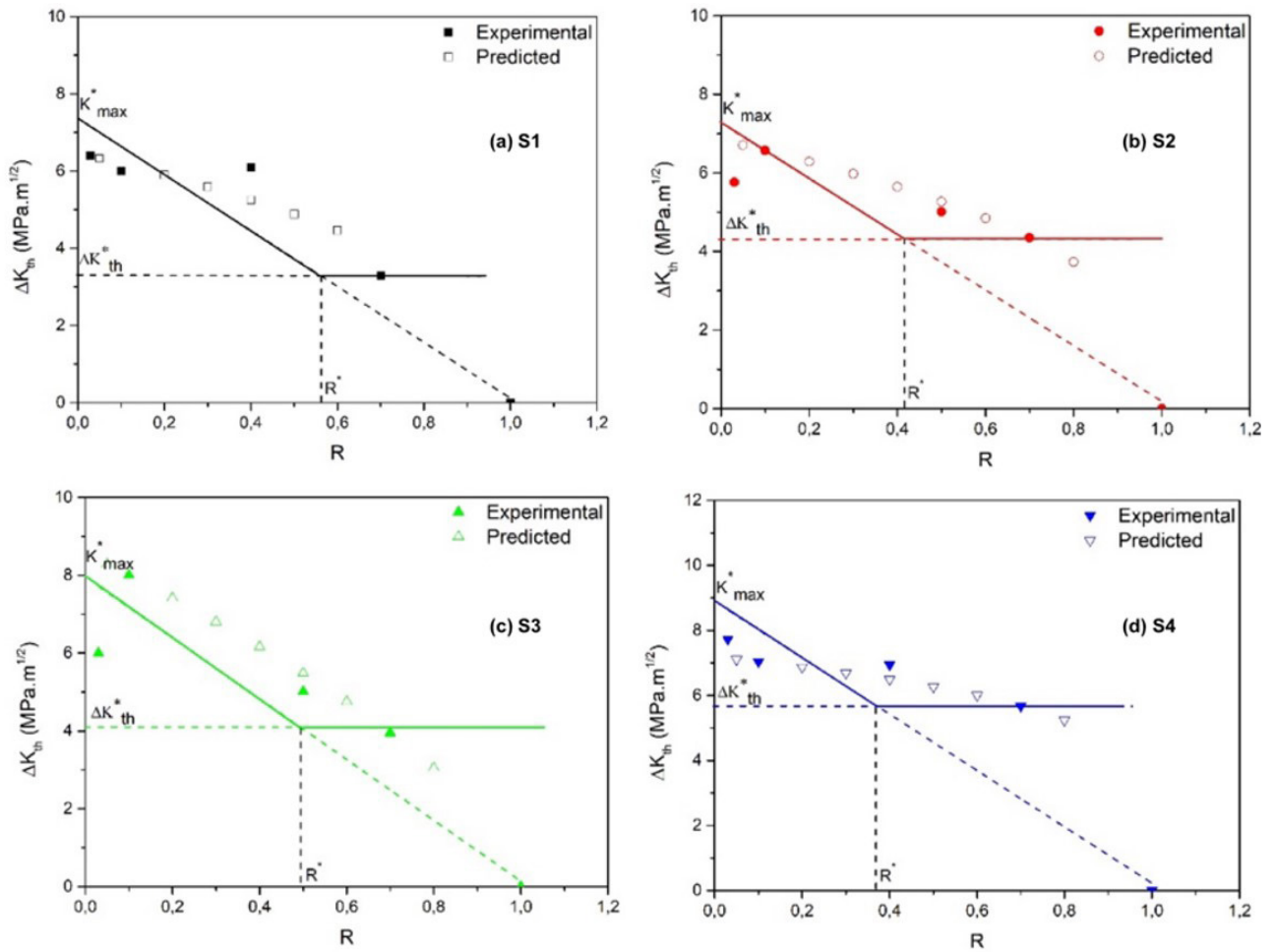


Figure 7. ΔK_{th} versus R curves. Vasudévan’s model.

Table 8. Values of ΔK_{th}^* and $K_{max,th}^*$ taken from Figure 6 for each steel. Modified crack closure model

Steel	ΔK_{th}^* (MPa.m ^{1/2})	$K_{max,th}^*$ (MPa.m ^{1/2})
S1	3.4	7.4
S2	4.3	7.3
S3	4.1	8.0
S4	5.7	8.9

Table 9. Values of the parameters of Equations 10 and 11 for all studied steels

Steel	a_2	b_2	c_2	a_3	b_3
S1	3.09056	-1.15768	0.334650	-0.79113	0.62275
S2	-3.77449	3.45082	0.578000	-0.32538	0.07594
S3	2.03444	-0.32676	0.269800	-1.01388	0.64041
S4	0.67745	0.43979	0.459940	-0.51312	0.35514

another important conclusion taken from the results shown in Figure 7 is that, based on the significance of R^* , the crack closure would cease to influence the FCG to a lower R value than expected. This fact seems to be a positive point for the general considerations proposed by Vasudevan and co-authors.

3.4 Application of the Zhu model

For the application of this model, it was considered $R_c = 0.7$, in the same way as in the previous models. The values of the coefficients of Equations 10 and 11 for each steel are presented in Table 9. According to Equation 8 and Equation 9, the predicted da/dN versus ΔK relationship is compared

with the experimental data, as shown in Figure 8 for all steels. It can be observed that the predicted curves agree reasonably well with the experimental fatigue data in the near-threshold region with a maximum error not more than 12%. This indicates that the prediction of FCG behavior from R of 0.03 to 0.7 is promising based on the proposed merged approach. The fatigue thresholds ΔK_{th} are also predicted when the value of $\Delta K_{th(0.7)}$ in Equation 9 is chosen at the da/dN of 1×10^{-7} mm/cyc. As indicated in Figure 9 and Table 10 for all steels, the fatigue thresholds from experiments are quite similar to those predicted by the model in Equation 8 and Equation 9. According to Zhu and co-authors’ model

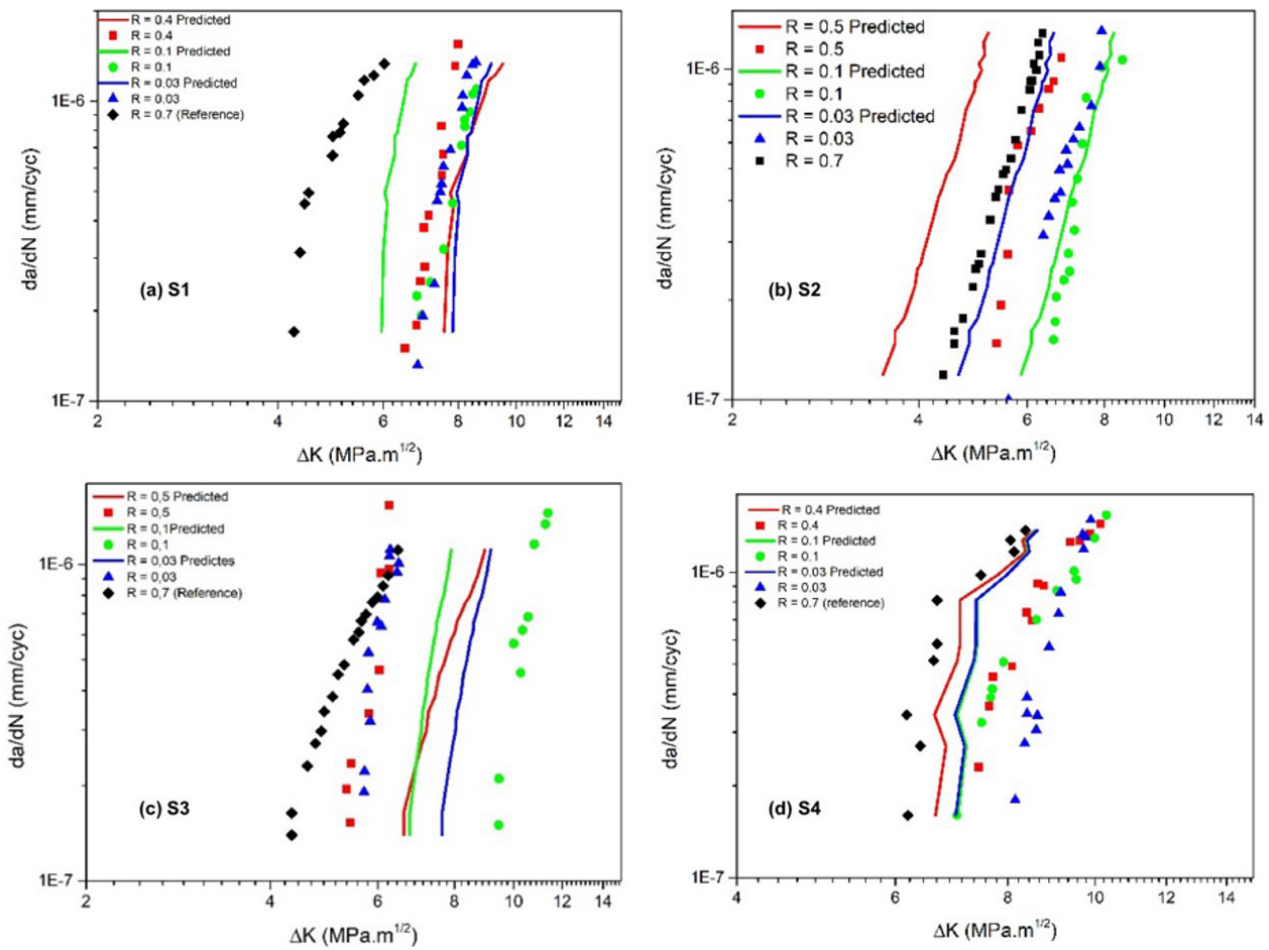


Figure 8. Comparison of experimental and predicted $da/dN \times \Delta K$ relationships in the near-threshold regime.

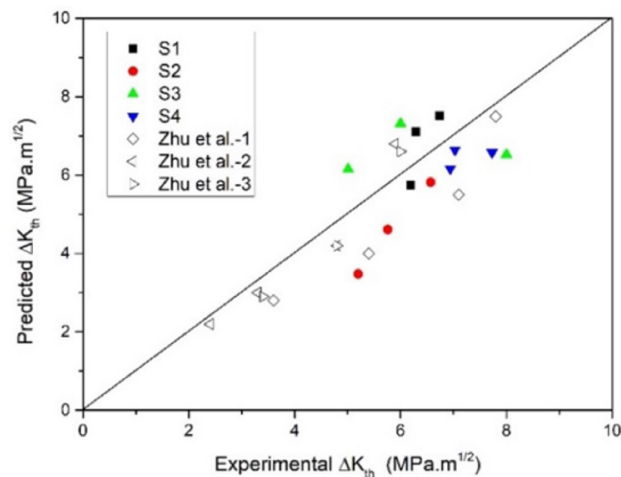


Figure 9. Predicted versus experimental fatigue thresholds for the studied steels and results from Zhu et al. [44] in a variety of Cr–Mo–V steels.

predictions, S4 steel has better performance in fatigue, followed by S3 for $R = 0.1$. However, it is important to note that some results have a deviation and that there is not an adequate prediction for the other R values. In order to reduce these

Table 10. Predicted versus experimental fatigue thresholds for the studied steels

Steel	R	Experimental ΔK_{th} (MPa.m ^{1/2})	Predicted ΔK_{th} (MPa.m ^{1/2})
S1	0.03/0.1/0.4/0.7	6.7/6.2/6.3/4.0	7.8/5.9/7.6/4.0
S2	0.03/0.1/0.5/0.7	5.8/6.6/5.2/4.3	4.6/6.0/3.5/4.3
S3	0.03/0.1/0.5/0.7	6.0/9.5/5.3/4.0	7.5/6.6/6.2/4.0
S4	0.03/0.1/0.4/0.7	7.7/7.0/6.9/5.7	6.9/7.0/6.6/5.7

Zhu and co-authors model.

errors, the complex mathematical manipulation would require the adoption of a greater range of values for the R -ratio, to imply a greater precision in the determination of the $A(R)$ and $B(R)$ functions, Equation 10 and Equation 11. Another aspect to consider is the choice of a more representative equation between da/dN and ΔK for the threshold region than the Paris equation.

Using the Zhu concepts, the experimental results were compared with the results obtained from the theoretical model, discussed above. In most of the cases, for the several samples and for different values of R , the datasets produce different results when performing linear fitting (using a

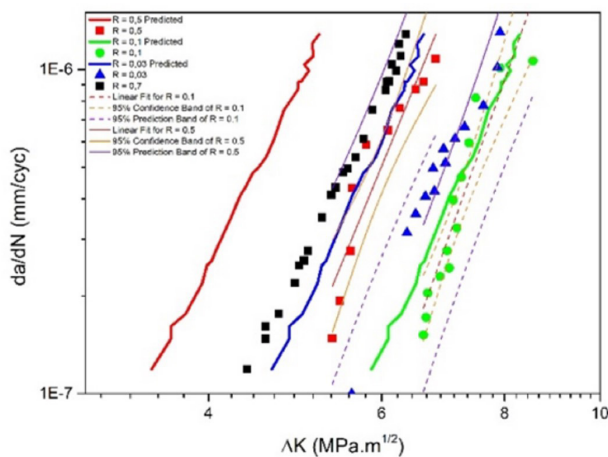


Figure 10. Linear Regression for S2 steel.

log-log scale). Points obtained through the theoretical model are not within the prediction bands of experimental fittings. Slopes and intercept coefficients are quite different, indeed. Therefore, it is not possible to conclude that the model proposed by Zhu can explain the experimental behavior. It is true that in few cases the Zhu model can be accepted, but those cases are exceptions.

As an example, see Figure 10. It represents the S2 steel. For green dots, representing $R = 0,1$, prediction bands for linear fitting (violet lines at right) contains the points obtained from the theoretical model. However, in contrast with this, prediction lines for $R = 0.5$ (red dots) are very far from points obtained from theoretical model (represented by the red line at left). This is the usual situation obtained in the comparison between experimental and theoretical results.

4 Conclusions

- Considering the chemical compositions, microstructures and mechanical tensile strength, as well as the international specifications currently adopted for automotive steels, S1 and S2 can be considered as HSLA ferrite/pearlite steels, the first type AISI 1010 and the second microalloyed to niobium. S3 and S4 are AHSS ferrite/bainite and ferrite/martensite steels,

respectively, the first microalloyed to niobium and the second with high chromium content.

- All steels presented the traditional sigmoidal curve of fatigue crack growth. The AHSS steels obtained the highest values for the threshold ΔK_{th} , being then more resistant to fatigue cracking than the HSLA steels. All four steels showed the same sensitivity to R -ratio, that is, decrease of fatigue strength with increase of R . The fracture mechanism was always the same, with tortuosity in the region close to the threshold and presence of striations at higher FCG rates.
- The manifestation of crack closure and its qualitatively expected dependence on the R -ratio were verified for the studied steels, but the Elber model was not able to provide a master curve that accurately summarized the effect of the R -ratio on the sigmoidal fatigue curve of steels.
- The combined use of two critical thresholds, ΔK_{th}^* and K_{max}^* , for predicting fatigue crack growth according to the Vasudevan model also did not provide accurate results in evaluating the effect of the R -ratio.
- The application of the methodology proposed by Zhu and coauthors, combining the two previous approaches, also provided a significant dispersion of results, once again failing to predict the effect of the R -ratio on the fatigue behavior of the steels.
- Considering that there is a connection between the two-parameter and crack closure models, the idea of Zhu and co-authors to link those methodologies is a promising alternative. However, experiments with a larger number of values for the R -ratio are needed, in order to have a more accurate expression among da/dN , ΔK and R . This research topic is still open, requiring a more in-depth phenomenological knowledge to predict the effect of the R ratio on fatigue crack growth.

Acknowledgements

T.F.M. would like to acknowledge CNPq/Brazil for financial support.

References

- Keeler S, Kimchi M, Mconey PJ, editors. Advanced high-strength steels: application guidelines - version 6.0. Middletown: WorldAutoSteel; 2017.
- Cooman BC, Findley K. Introduction to the mechanical behavior of steel. Warrendale: Association for Iron & Steel Technology; 2017.
- Fonstein N. Advanced high strength sheet steels. Cham: Springer; 2015.
- Suzuki H, McEvily AJ. Microstructural effects on fatigue crack growth in a low carbon steel. Metallurgical Transactions. 1979;10:475-481.

- 5 Minakawa K, Matsuo Y, McEvily AJ. The influence of a duplex microstructure in steels on fatigue crack growth in the near-threshold region. *Metallurgical Transactions*. 1982;13:439-445.
- 6 Dutta VB, Suresh S, Ritchie RO. Fatigue crack propagation in dual-phase steels. *Metallurgical Transactions*. 1984;15:1193-1207.
- 7 Wasynczuk JA, Ritchie RO, Thomas G. Effects of microstructure on fatigue crack growth in duplex ferrite-martensite steels. *Materials Science and Engineering*. 1984;62:79-92.
- 8 Tzou JL, Ritchie RO. Fatigue crack propagation in a dual-phase plain-carbon steel. *Scripta Metallurgica*. 1985;19:751-755.
- 9 Ramage RM, Jata KV, Shiflet GJ, Starke EA. The effect of phase continuity on the fatigue and crack closure behavior of a dual-phase steel. *Metallurgical Transactions*. 1987;18:1291-1298.
- 10 Sun L, Li S, Zang Q, Wang Z. Dependence of fatigue crack closure behaviour on volume fraction of martensite in dual-phase steels. *Scripta Metallurgica*. 1995;32:517-521.
- 11 Sarwar M, Priestner R. Fatigue crack propagation behaviour in dual-phase steel. *Journal of Materials Engineering and Performance*. 1999;8:245-251.
- 12 Gritti JA, Melo TMF, Machado FA, Horta WS, Cândido LC, Godefroid LB. Influência da pré-deformação e do tratamento de “*bake hardening*” na tenacidade à fratura e na resistência à fadiga de dois aços bifásicos. In: *Anais do 61º Congresso Anual da ABM; 2006; Rio de Janeiro, Brasil*. São Paulo: ABM; 2006.
- 13 Cheng X, Petrov R, Zhao L, Janssen M. Fatigue crack growth in TRIP steel under positive R-ratios. *Engineering Fracture Mechanics*. 2008;75:739-749.
- 14 Gutz AE, Machado FA, Gritti JA, Melo TMF, Cândido LC, Godefroid LB. Tenacidade à fratura e resistência ao crescimento de trinca por fadiga de um aço bifásico da classe de 780MPa de resistência. In: *Anais do 65º Congresso Anual da ABM; 2010; Rio de Janeiro, Brasil*. São Paulo: ABM; 2010.
- 15 Godefroid LB, Andrade MS, Horta WS, Machado FA. Effect of prestrain and bake hardening heat treatment on fracture toughness and fatigue crack growth resistance of two dual-phase steels. In: *Proceedings of the Materials Science and Technology Conference; 2011; Columbus OH, USA*. Warrendale: Association for Iron & Steel Technology; 2011.
- 16 Idris R, Prawoto Y. Influence of ferrite fraction within martensite matrix on fatigue crack propagation: an experimental verification with dual phase steel. *Materials Science and Engineering*. 2012;A552:547-554.
- 17 Guan M, Yu H. Fatigue crack growth behaviors in hot-rolled low carbon steels: a comparison between ferrite-pearlite and ferrite-bainite microstructures. *Materials Science and Engineering A*. 2013;559:875-881.
- 18 Li S, Kang Y, Kuang S. Effects of microstructure on fatigue crack growth behavior in cold-rolled dual phase steels. *Materials Science and Engineering*. 2014;A612:153-161.
- 19 Godefroid LB, Lima APS, Vilela TCG, Martins CA, Fonstein N. Effect of Mo and Cr on the fracture toughness and fatigue crack growth resistance of a complex-phase Cr-Mn-V steel. In: *Proceedings of the 23rd ABCM International Congress of Mechanical Engineering (COBEM); 2015; Rio de Janeiro, RJ, Brasil*. Rio de Janeiro: ABCM; 2015.
- 20 Anderson TL. *Fracture mechanics: fundamentals and applications*. Boca Raton: CRC Press; 2017.
- 21 Paris PC, Erdogan F. A critical analysis of crack propagation laws. *Journal of Basic Engineering*. Transactions of the American Society of Mechanical Engineers. 1963;85:528-534.
- 22 Ritchie RO. Near-threshold fatigue-crack propagation in steels. *International Metallurgical Reviews*. 1979;24:205-230.
- 23 Liaw PK, Leax TR, Logsdon WA. Near-threshold fatigue crack growth behavior in metals. *Acta Metallurgica*. 1983;31:1581-1587.
- 24 El-Shabasy AB, Lewandowski JJ. Effects of load ratio R and temperature on fatigue crack growth of fully pearlitic eutectoid steel. *International Journal of Fatigue*. 2004;26:305-309.
- 25 Godefroid LB, Moreira LP, Vilela TCG, Faria GL, Candido LC, Pinto ES. Effect of chemical composition and microstructure on the fatigue crack growth resistance of pearlitic steels for railroad application. *International Journal of Fatigue*. 2019;120:241-253.
- 26 Stanzl-Tschegg SE, Plasser O, Tschegg EK, Vasudevan AK. Influence of microstructure and load ratio on fatigue threshold behavior in 7075 aluminum alloy. *International Journal of Fatigue*. 1991;21:255-262.
- 27 Godefroid LB, Barroso EKL, Al-Rubaie KS. Fatigue crack growth analysis of pre-strained 7475-T7351 aluminum alloy. *International Journal of Fatigue*. 2006;28:934-942.

- 28 Al-Rubaie KS, Barroso EKL, Godefroid LB. Statistical modeling of fatigue crack growth rate in pre-strained 7475-T7351 aluminium alloy. *Materials Science and Engineering A*. 2008;486:585-595.
- 29 Jones R, Molent L, Walker K. Fatigue crack growth in a diverse range of materials. *International Journal of Fatigue*. 2012;40:43-50.
- 30 Dubey S, Soboyejo ABO, Soboyejo WO. An investigation of the effects of stress ratio and crack closure on the micromechanisms of fatigue crack growth in Ti-6Al-4V. *Acta Materialia*. 1997;45:2777-2787.
- 31 Boyce BL, Ritchie RO. Effect of load ratio and maximum stress intensity on the fatigue threshold in Ti-6Al-4V. *Engineering Fracture Mechanics*. 2001;68:129-147.
- 32 Godefroid LB, Lopes J, Al-Rubaie KS. Statistical modeling of fatigue crack growth rate in Inconel alloy 600. *International Journal of Fatigue*. 2007;29:931-940.
- 33 Roy AK, Pal J, Hasan MH. Temperature and load ratio effects on crack-growth behavior of austenitic superalloys. *Journal of Engineering Materials and Technology*. 2010;132(1):1-7.
- 34 Zhihong Z, Yuefeng G, Osada T, Yong Y, Chuanyong C, Yokokawa T, et al. Fatigue crack growth characteristics of a new Ni-Co-base superalloy TMW-4M3: effects of temperature and load ratio. *Journal of Materials Science*. 2011;46:7573-7581.
- 35 Elber W. Fatigue crack closure under cyclic tension. *Engineering Fracture Mechanics*. 1970;2:37-45.
- 36 Elber W. The significance of fatigue crack closure. In: American Society for Testing and Materials – ASTM, editor. *Damage tolerance in aircraft structures – ASTM STP 486*. West Conshohocken: ASTM International; 1971. p. 230-242.
- 37 Hudak SJ, Davidson DL. The dependence of crack closure on fatigue loading variables. In: American Society for Testing and Materials – ASTM, editor. *Mechanics of fatigue crack closure, ASTM STP 982*. West Conshohocken: ASTM International; 1988. p. 121-138.
- 38 Vasudevan AK, Sadananda K, Louat N. A review of crack closure, fatigue crack threshold and related phenomena. *Materials Science and Engineering A*. 1994;188:1-22.
- 39 Sadananda K, Vasudevan AK, Holtz RL. Extension of the unified approach to fatigue crack growth to environmental interactions. *International Journal of Fatigue*. 2001;23:277-286.
- 40 Sadananda K, Vasudevan AK. Fatigue crack growth mechanisms in steels. *International Journal of Fatigue*. 2003;25:899-914.
- 41 Sadananda K, Vasudevan AK. Crack tip driving forces and crack growth representation under fatigue. *International Journal of Fatigue*. 2004;26(1):39-47.
- 42 Vasudevan AK, Sadananda K, Iyyer N. Fatigue damage analysis: Issues and challenges. *International Journal of Fatigue*. 2016;82:120-133.
- 43 Zhu ML, Xuan FZ, Tu ST. Interpreting load ratio dependence of near-threshold fatigue crack growth by a new crack closure model. *International Journal of Pressure Vessels and Piping*. 2013;110:9-13.
- 44 Zhu ML, Xuan FZ, Tu ST. Effect of load ratio on fatigue crack growth in the near-threshold regime: a literature review, and a combined crack closure and driving force approach. *Engineering Fracture Mechanics*. 2015;141:55-77.
- 45 De AK, Speer JG, Matlock DK. Color tint-etching of multi-phase steels. *Advanced Materials & Processes*. 2003;161(2):27-30.
- 46 American Society for Testing and Materials – ASTM. ASTM E112: standard test methods for determining average grain size. West Conshohocken: ASTM International; 2013.
- 47 American Society for Testing and Materials – ASTM. ASTM E8 M: standard test methods for tension testing of metallic materials. West Conshohocken: ASTM International; 2016.
- 48 American Society for Testing and Materials – ASTM. ASTM E 92: standard test methods for Vickers hardness and Knoop hardness of metallic materials. West Conshohocken: ASTM International; 2017.
- 49 American Society for Testing and Materials – ASTM. ASTM E647-15: standard test method for measurement of fatigue crack growth rates. West Conshohocken: ASTM International; 2016.
- 50 Klesnil M, Lukáš P. *Fatigue of metallic materials*. Prague: Elsevier Science; 1992.
- 51 Dasarathy C, Goodwin TJ. Recent developments in automotive steels. *Metals and Materials*. 1990;6:21-28.

- 52 Abdalla AJ, Hashimoto TM, Moura NCM, Pereira MS, Souza NS, Mendes FA. Alterações das propriedades mecânicas em aços 4340 e 300M através de tratamentos térmicos isotérmicos e intercríticos. In: Anais do 59º Congresso Anual da ABM; 2004; São Paulo, Brasil. São Paulo: ABM; 2004.
- 53 Klaus H, Friedrich H. Low carbon structural steels: the key to economic constructions. In: Proceedings of the Symposium on Low Carbon Steels for the 90's; 1993; Pittsburg; USA. Warrendale: Metals & Mat. Soc.; 1993. p. 211-218.
- 54 Mecelis GR, Assis CLR, Gallego J. Relação de Hall-Petch em aços microligados produzidos como tiras a quente. In: Anais do 22º Congresso Brasileiro de Engenharia e Ciência dos Materiais; 2016; Natal, Brasil. São Paulo: Metallum Congressos Técnicos e Científicos; 2016. p. 4824-4833.
- 55 Podder AS, Pandit A, Murugaiyan A, Bhattacharjee D, Ray RK. Phase transformation behaviour in two C–Mn–Si based steels under different cooling rates. *Ironmaking & Steelmaking*. 2007;34(1):83-88.
- 56 Rigsbee JM, VanderArendt PJ. Laboratory studies of microstructures and structure-properties relationships in dual-phase HSLA steels. In: Davenport AT, editor. *Formable HSLA and dual-phase steels*. Warrendale: AIME; 1979. p. 56-86.
- 57 Tanaka T, Nishida M, Hashiguchi K, Kato T. Formation and properties of ferrite plus martensite dual-phase structures. In: *Structure and Properties of Dual-Phase Steels*; 1979; New Orleans, LA. Warrendale: AIME; 1979. p. 221-241.
- 58 Rashid MS, Rao BVN. Tempering characteristics of a vanadium containing dual-phase steel. In: *Proceedings of the Fundamentals of Dual-Phase Steels*; 1981; Chicago, IL. Warrendale: AIME, 1981, p. 249-264.
- 59 Matlock DK, Zia-Ebrahimi F, Krauss G. Deformation, processing and structure. Materials Park: ASM; 1984. *Structure, properties and strain hardening of dual-phase steels*; p. 47-87.
- 60 Krauss G. *Steels: processing, structure and performance*. 2nd ed. Materials Park: ASM International; 2005. p. 250-256.

Received: 30 Jun. 2022

Accepted: 28 Mar. 2023